Collapse Analysis for Elliptic Cones

B. O. Almroth,* F. A. Brogan,† and M. B. Marlowe‡
Lockheed Palo Alto Research Laboratory, Palo Alto, Calif.

An analysis based on the nonlinear equations for a general shell has been programed for computer solution. The computer program was applied in a study of the collapse of elliptic cylinders and cones under axial compression. A two-dimensional finite difference approach was used for the numerical analysis. The grid lines follow the shell boundaries which necessitates the use of nonorthogonal surface coordinates. The shells were subjected to a uniform axial end shortening, and it was found that for shells of this type, under this loading condition, the load-displacement curves exhibited more than one maximum. The secondary buckling loads were found to be only moderately sensitive to shell imperfections and could be suitable as design limits.

Nomenclature

A,B,C = coefficients of first fundamental form [Eq. (8)]
A = matrix $[A_{jk} = \partial^2 U/(\partial X_j \partial X_k)]$
D = $Et/(1 - \nu^2)$
D^2 = see Eq. 15
D^i = matrix of constants [Eq. (27)]
E = Young's modulus
F = vector of external forces
H = see Eq. (26)
K = $Et^3/[12(1 - \nu^2)]$
L = nonlinear operator [Eq. (31)]
m = number of mesh points
S^i = stress resultants at mesh station i
ds = surface area element
U = strain energy
ΔU^i = strain energy density at mesh station i
V = total potential energy
W = work done by external forces
X,Y,Z = Cartesian coordinates
X_i = displacement components
Z^i = strains and curvature changes at mesh station i
Z^{i*} = transpose of matrix Z^i
$\bar{a},\bar{b},c,d$ = parameters for elliptic cone
a,b = $\bar{a}/c$ and $\bar{b}/c$, respectively
a^i = area of subregion surrounding mesh station i
$a_{\alpha\beta}$ = metric tensor
$b_{\alpha\beta}$ = coefficient of second fundamental form (curvature tensor)
$\mathbf{n}$ = normal vector to shell surface (X,Y,Z)
$\mathbf{r}$ = radius vector to point on shell surface (X,Y,Z)
t = shell thickness
u,v = physical components of in-plane displacements
w = normal displacement
w_0 = initial imperfection amplitude
ξ = w_0/t
x,y = surface coordinates
$\Gamma_{\alpha\beta}{}^{\rho}$ = Christoffel symbols
Ω = out-of-plane rotation
θ = angle between surface coordinates
α,β = surface coordinates
β_α = displacement gradients [Eq. (2)]
$\gamma_{\alpha\beta}$ = displacement gradients [Eq. (2)]
$\epsilon_{\alpha\beta}$ = middle surface strain tensor
$\varkappa_{\alpha\beta}$ = curvature-change tensor
ν = Poisson's ratio
φ = angular coordinate

Introduction

FOR shells of more general shape than the shell of revolution, it is not possible to separate the governing partial differential equations with respect to the spatial coordinates. The analysis thus requires the use of two independent space variables, and the numerical analysis is drastically encumbered. In addition, if the collapse load of the shell is to be determined one must cope with a nonlinear analysis. Finite-difference methods[1] as well as finite-element methods[2] have been used in such analyses. While the finite-element approach is more widely applicable, it appears that a finite-difference solution is less expensive in terms of computer time. Thus the finite-difference method should be preferred whenever it is applicable, i.e., for cases in which the shell surface as well as a suitable system of surface coordinates can be mathematically defined.

For an elliptic cone (Fig. 1) it is easy to form analytical expressions for the shell midsurface and for a set of grid lines composed of the straight line generators and the intersections with planes perpendicular to the shell axis. Therefore, the solution of the collapse problem was obtained here through extension of the finite-difference analysis of Ref. 1 and through modification of the corresponding computer program (STAGS).

The surface coordinate lines which form the finite difference grid follow the shell boundaries which greatly facilitates a finite-difference analysis. However, since they are not orthogonal, the basic equations are considerably more complicated than those of Ref. 1. The energy expression is derived here in terms of physical components of displacement for a general shell configuration with nonorthogonal coordinates. The derivation is based on the tensor formulation.[3] The constants which appear in the expression for the strain energy are determined as functions of the shell coordinates for the special case of an elliptic cone. Numerical results are presented for the collapse of elliptic cylinders as well as for elliptic cones.

Governing Equations

The expressions for strain and curvature change used here are[3]

$$\epsilon_{\alpha\beta} = \tfrac{1}{2}(\gamma_{\alpha\beta} + \gamma_{\beta\alpha}) + \tfrac{1}{2}\beta_\alpha\beta_\beta + \tfrac{1}{2}\gamma_{\rho\alpha}\Sigma\cdot{}^{\rho}{}_{\beta}$$
$$\varkappa_{\alpha\beta} = \beta_{\beta|\alpha} + b_\alpha{}^{\rho}\gamma_{\rho\beta} + b_{\alpha\beta}\gamma\cdot{}^{\rho}{}_{\rho} \qquad (1)$$

where $\gamma_{\alpha\beta}$ and β_α are the displacement gradients defined by

$$\gamma_{\alpha\beta} = u_{\alpha|\beta} - b_{\alpha\beta}w \qquad (2)$$
$$\beta_\alpha = w_{,\alpha} + b_\alpha{}^{\beta}u_\beta \qquad (3)$$

The curvature tensor $b_{\alpha\beta}$ is defined with respect to the inner normal vector. A bar (|) denotes covariant differentiation, and a comma (,) denotes partial differentiation with respect to the coordinates of the shell. The choice of Eqs. (1) is based upon the assumption that the rotation about the normal

Received January 5, 1970; revision received June 12, 1970. The research work presented here was in part sponsored by the Air Force Flight Dynamics Laboratory, Wright-Patterson Air Force Base, Ohio under Contract F33615-69-C-1523.

* Senior Staff Scientist. Member AIAA.
† Research Scientist.
‡ Research Scientist. Member AIAA.

is of the same order of magnitude as the square root of a typical middle surface strain, and that the out of plane rotation ($\Omega^2 \equiv \beta_\alpha\beta^\alpha$) can be moderately large ($\Omega \approx 18°$).

While the strain tensor used is a standard expression, the curvature change tensor is not well known. This tensor differs from Sander's[4] curvature change tensor in that it is valid for much larger out-of-plane rotations. A complete and rigorous derivation is given in Ref. 3.

The strain energy expression in tensor form is

$$U = \tfrac{1}{2}(E/1 - \nu^2)[(1 - \nu)a^{\alpha\beta}a^{\beta\lambda} + \nu a^{\alpha\rho}a^{\beta\lambda}] \times [t\epsilon_{\alpha\rho}\epsilon_{\beta\lambda} + (t^3/12)\varkappa_{\alpha\rho}\varkappa_{\beta\lambda}] \quad (4)$$

The physical components of displacements in terms of the contravarient components, with the surface coordinates denoted by x and y, are

$$u = (a_{xx})^{1/2}u^x,\ v = (a_{yy})^{1/2}u^y \quad (5)$$

The covariant components are

$$u_x = (a_{xx})^{1/2}u + (a_{xy})/(a_{xy})^{1/2}v,$$
$$u_y = (a_{xy})/(a_{xx})^{1/2}u + (a_{yy})v \quad (6)$$

By use of Eqs. (1–6) the energy can be expressed in terms of the physical components of displacement. For the strain energy we obtain the following form

$$\begin{aligned} U = (D/2)\{&(A\sin\theta)^{-4}\epsilon_x{}^2 - (4A\cos\theta/B)(A\sin\theta)^{-4}\epsilon_x\epsilon_{xy} + \\ &2[1 - (1 - \nu)\sin^2\theta](AB\sin^2\theta)^{-2}\epsilon_x\epsilon_y + \\ &2(AB\sin^2\theta)^{-2}[(1 - \nu) + (1 + \nu)\cos^2\theta]\epsilon_{xy}{}^2 - \\ &(4B\cos\theta/A)(B\sin\theta)^{-4}\epsilon_{xy}\epsilon_y + (B\sin\theta)^{-4}\epsilon_y{}^2\} + \\ (K/2)\{&(A\sin\theta)^{-4}\varkappa_x{}^2 - (4A\cos\theta/B)(A\sin\theta)^{-4}\varkappa_x\varkappa_{xy} + \\ &2[1 - (1 - \nu)\sin^2\theta](AB\sin^2\theta)^{-2}\varkappa_x\varkappa_y + \\ &2(AB\sin^2\theta)^{-2}[(1 - \nu)\cos^2\theta]\varkappa_{xy}{}^2 - (4B\cos\theta/A) \times \\ &(B\sin\theta)^{-4}\varkappa_{xy}\varkappa_y + (B\sin\theta)^{-4}\varkappa_y{}^2\} \end{aligned} \quad (7)$$

Here A,B are the coefficients of the first fundamental form, and θ represents the angle between the surface coordinate lines.

$$I = A^2dx^2 + 2AB(\cos\theta)dxdy + B^2dy^2 = ds^2 \quad (8)$$

The covariant form of the membrane strain components is expressed in terms of the displacement components through the following relations

$$\begin{aligned} \epsilon_x &= \gamma_{xx} + \tfrac{1}{2}(\beta_x{}^2 + \gamma_{xx}\gamma_{\cdot x}{}^x + \gamma_{yx}\gamma_{\cdot x}{}^y) \\ \epsilon_{xy} &= \tfrac{1}{2}(\gamma_{yx} + \gamma_{xy} + \beta_x\beta_y + \gamma_{xx}\gamma_{\cdot y}{}^x + \gamma_{yx}\gamma_{\cdot y}{}^y) \\ \epsilon_y &= \gamma_{yy} + \tfrac{1}{2}(\beta_y{}^2 + \gamma_{xy}\gamma_{\cdot y}{}^x + \gamma_{yy}\gamma_{\cdot y}{}^y) \end{aligned} \quad (9)$$

where

$$\beta_x = w_{,x} + (b_{xx}/A)u + (b_{xy}/B)v$$
$$\beta_y = w_{,y} + (b_{xy}/A)u + (b_{yy}/B)v \quad (10)$$

$$\begin{aligned} \gamma_{xx} &= Au_{,x} + A/B(A_{,y} - B_{,x}\cos\theta)v + A\cos\theta v_{,x} - b_{xx}w \\ \gamma_{xy} &= Au_{,y} + [(A\cos\theta)_{,y} - B_{,x}]v + A\cos\theta v_{,y} - b_{xy}w \\ \gamma_{yx} &= [(B\cos\theta)_{,x} - A_{,y}]u + B\cos\theta\, u_{,x} + Bv_{,x} - b_{xy}w \\ \gamma_{yy} &= B/A(B_{,x} - A_{,y}\cos\theta)u + B\cos\theta\, u_{,y} + Bv_{,y} - b_{yy}w \\ \gamma_{\cdot x}{}^x &= 1/A\, u_{,x} + [\cos\theta/(AB\sin^2\theta)][A_{,y} - (B\cos\theta)_{,x}]u + \\ &\quad [1/(AB\sin^2\theta)][A_{,y} - \cos\theta\, B_{,x}]v - b_x{}^x w \\ \gamma_{\cdot y}{}^x &= 1/A\, u_{,y} + [1/(A^2\sin^2\theta)][(A\cos\theta)_{,y} - B_{,x}]v + \\ &\quad [\cos\theta/(A^2\sin^2\theta)][A_{,y}\cos\theta - B_{,x}]u - b_y{}^x w \\ \gamma_{\cdot x}{}^y &= 1/B\, v_{,x} + [1/(B^2\sin^2\theta)][B\cos\theta,x - A_{,y}]u + \\ &\quad [\cos\theta/(B^2\sin^2\theta)][B_{,x}\cos\theta - A_{,y}]v + b_x{}^y w \\ \gamma_{\cdot y}{}^y &= 1/B\, v_{,y} + [\cos\theta/(AB\sin^2\theta)][B_{,x} - (A\cos\theta)_{,y}]v + \\ &\quad [1/(AB\sin^2\theta)][B_{,x} - \cos\theta\, A_{,y}]u - b_y{}^y w \end{aligned} \quad (11)(12)$$

Here b_{xx}, b_{xy}, and b_{yy} are the coefficients of the second fundamental form defined by

$$II = b_{xx}d_x{}^2 + 2b_{xy}dxdy + b_{yy}dy^2 \quad (13)$$

and

$$\begin{aligned} b_x{}^x &= [1/(A^2\sin^2\theta)]b_{xx} - [\cos\theta/(AB\sin^2\theta)]b_{xy} \\ b_x{}^y &= [1/(B^2\sin^2\theta)]b_{xy} - [\cos\theta/(AB\sin^2\theta)]b_{xx} \\ b_y{}^x &= [1/(A^2\sin^2\theta)]b_{xy} - [\cos\theta/(AB\sin^2\theta)]b_{yy} \\ b_y{}^y &= [1/(B^2\sin^2\theta)]b_{yy} - [\cos\theta/(AB\sin^2\theta)]b_{xy} \end{aligned} \quad (14)$$

The covariant components of the changes of curvature are

$$\varkappa_x = \beta_{x,x} - \Gamma_{xx}{}^x\beta_x - \Gamma_{xx}{}^y\beta_y + b_{xy}\gamma_{\cdot x}{}^y - b_{xx}\gamma_{\cdot y}{}^y$$
$$\varkappa_{xy} = \tfrac{1}{2}[\beta_{x,y} - \Gamma_{xy}{}^x\beta_x - \Gamma_{xy}{}^y\beta_y + \beta_{y,x} - \Gamma_{xy}{}^x\beta_x - \Gamma_{xy}{}^y\beta_y + b_{xx}\gamma_{\cdot y}{}^x + b_{yy}\gamma_{\cdot x}{}^y - b_{xy}\gamma_{\cdot x}{}^x - b_{xy}\gamma_{\cdot y}{}^y]$$
$$\varkappa_y = \beta_{y,y} - \Gamma_{yy}{}^y\beta_y - \Gamma_{yy}{}^x\beta_x + b_{xy}\gamma_{\cdot y}{}^x - b_{yy}\gamma_{\cdot x}{}^x$$

with

$$C = AB\cos\theta,\ D^2 = AB\sin^2\theta \quad (15)$$

the Christoffel symbols are defined by

$$\begin{aligned} \Gamma_{xx}{}^x &= [BA_{,x} + (AA_{,y} - C_{,x})\cos\theta]/D^2 \\ \Gamma_{xx}{}^y &= (A/B)[C_{,x} - BA_{,x}\cos\theta - AA_{,y}]/D^2 \\ \Gamma_{xy}{}^x &= [BA_{,y} - BB_{,x}\cos\theta]/D^2 \\ \Gamma_{xy}{}^y &= [AB_{,x} - AA_{,y}\cos\theta]/D^2 \\ \Gamma_{yy}{}^x &= (B/A)[C_{,y} - BB_{,x} - AB_{,y}\cos\theta]/D^2 \\ \Gamma_{yy}{}^y &= [AB_{,y} - (BB_{,x} - C_{,y})\cos\theta]/D^2 \end{aligned} \quad (16)$$

The geometry of an elliptic cone is shown in Fig. 1. The shell surface and its boundaries are defined by the distances $\bar{a}$, $\bar{b}$, c, and d. The geometrical constants occurring in the kinematic relations are most conveniently determined if elliptic coordinates are used in the definition of the shell midsurface. If x and y are elliptical surface coordinates and X,Y,Z are the coordinates in a Cartesian system

$$X = ax\cos y,\ Y = bx\sin y,\ Z = x \quad (17)$$

where

$$a = \bar{a}/c,\ b = \bar{b}/c \quad (18)$$

The surface coordinate x represents the distance from the apex of the cone and y can be expressed in terms of the angular coordinate φ through

$$y = \arctan[(a/b)\tan\varphi] \quad (19)$$

Let $\mathbf{r}$ represent the radius vector in the X,Y,Z system to a point on the shell surface. Then, the coefficients in the first fundamental form are

$$A = \mathbf{r}_{,x}\cdot\mathbf{r}_{,x},\ C = \mathbf{r}_{,x}\cdot\mathbf{r}_{,y},\ B = \mathbf{r}_{,y}\cdot\mathbf{r}_{,y} \quad (20)$$

The coordinate lines intersect one another in an angle

$$\theta = \arccos[C/(AB)] \quad (21)$$

Substitution of Eqs. (17) into Eqs. (20) yields

$$\begin{aligned} A &= (1 + a^2\cos^2y + b^2\sin^2y)^{1/2} \\ C &= -x(a^2 - b^2)\sin y\cos y \\ B &= x(a^2\sin^2y + b^2\cos^2y)^{1/2} \end{aligned} \quad (22)$$

The derivatives of these coefficients are

$$\begin{aligned} A_{,x} &= 0,\ C_{,x} = C/x,\ B_{,x} = B/x \\ A_{,y} &= -(a^2 - b^2)\sin y\cos y/(2A) \\ C_{,y} &= -x(a^2 - b^2)(\cos^2y - \sin^2y) \\ B_{,y} &= x^2\sin y\cos y(a^2 - b^2)/B \end{aligned} \quad (23)$$

The normal to the surface is defined by

$$\mathbf{n} = (\mathbf{r}_{,x} \times \mathbf{r}_{,y})/(AB \sin\theta) \tag{24}$$

and the coefficients in the second fundamental form are obtained from

$$b_{xx} = \mathbf{r}_{,xx}\cdot\mathbf{n},\ b_{xy} = \mathbf{r}_{,xy}\cdot\mathbf{n}$$
$$b_{yy} = \mathbf{r}_{,yy}\cdot\mathbf{n} \tag{25}$$

Through substitution of Eqs. (17) into Eq. (25) these coefficients and their derivatives are determined

$$b_{xx} = b_{xy} = 0,\ b_{xx,x} = b_{xy,y} = 0$$
$$b_{xx,y} = b_{xy,y} = 0,\ b_{yy} = -abx^2/H$$
$$b_{yy,x} = b_{yy}/x \tag{26}$$
$$b_{yy,y} = abx(x^3/H)\ \text{siny cosy}(a^2 - b^2)$$

where

$$H = x(a^2 \sin^2 y + b^2 \cos^2 y + a^2b^2)^{1/2}$$

Numerical Method

The numerical solution is based upon a two-dimensional finite-difference approximation. The shell surface is covered with mesh lines parallel to the coordinate lines, and the unknowns of the system are the normal displacements w at the grid points and the tangential displacements u and v at points between adjacent grid points.

After replacement of the displacements and their derivatives in Eq. (7) by finite-difference approximations, the strain energy density at mesh station i can be written in the form

$$\Delta U^i = \tfrac{1}{2} Z^{i*} D^i Z^i \tag{27}$$

where D^i is a 6×6 positive definite matrix of constants and Z^i is the vector of strain and curvature changes at station i. D^i and Z^i are functions of the geometric parameters of the shell; in addition, D^i is dependent on the material properties. The vector of stress resultants at station i is given by

$$S^i = D^i Z^i \tag{28}$$

ΔU^i is a 4th-order polynomial in the displacement components since the components of Z^i are either linear or quadratic expressions in the displacement components.

The total potential energy V of the shell is obtained by combination of the strain energy and the work done by the external forces

$$V = U - W$$

where

$$U = \sum_i^m \Delta U^i \cdot a^i \tag{29}$$

and

$$W = X^* \cdot F$$

Here X denotes the vector of displacement components, F is the vector of external forces, and a^i is the area of the ith subregion. A necessary condition for static equilibrium is that the total potential energy has a minimum. This condition requires the vanishing of the first variation of V and leads to the equation

$$LX = F \tag{30}$$

where the operator L is defined by

$$LX = \text{Grad } U \tag{31}$$

L is thus a nonlinear "stiffness" operator which relates displacement components and external forces.

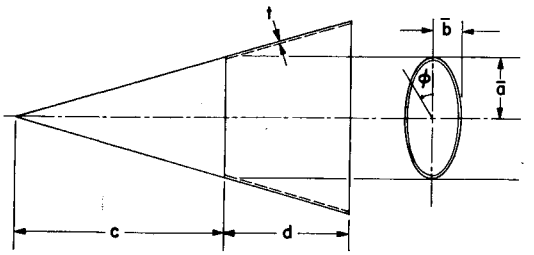

Fig. 1 Elliptic cone.

The computation of LX and A is facilitated by a decomposition of the operator L corresponding to the mesh stations

$$L = \sum_i^m L^i \tag{32}$$

where $L^iX = \text{Grad } U^i \cdot a^i$.

For shells with noncircular cross section the bifurcation buckling theory is not applicable, since the deformation pattern prior to collapse in general already contains a component of the buckling mode which develops at collapse. The present version of the STAGS program does not consider bifurcation buckling, and the results presented here were based on a complete nonlinear analysis. Possible bifurcation must, however, be considered with respect to any mode which is orthogonal to the primary deformation mode.

For the particular cases of the elliptic cylinder and the elliptic cone, there are planes of symmetry with respect to geometry as well as loading. Hence, bifurcation is possible into modes which are antisymmetric with respect to these planes. In order to make it possible to predict such bifurcation, the effects of initial geometrical displacements were included in the program. If a small imperfection is present which is antisymmetric with respect to the symmetry planes, the antisymmetric buckling pattern will develop rapidly as the corresponding buckling load is approached.

Inclusion of geometric imperfections is important also because the critical load of many shells is sensitive to such imperfections. Consequently, Eqs. (9) were modified to include small values of the initial displacement $\bar{w}$. The terms $\bar{w}_x\beta_x$, $\bar{w}_y\beta_y$, and $\bar{w}_x\beta_y + {}_y\bar{w}\beta_x$ were added to the three middle surface strains ϵ_x, ϵ_y, and ϵ_{xy}.

Numerical Results

Numerical results were first obtained for an elliptic cylinder with a length of 1.0 in., a thickness of 0.0144 in., and semiaxes of 1.75 in. and 1.0 in. Young's modulus was 10^7 psi, and Poisson's ratio was 0.3. The cylinder was subjected to a uniform end shortening with the edges free to rotate but restrained from moving in the radial and circumferential directions.

Since the "buckling pattern" was expected to be confined to the areas of least curvature it appeared that antisymmetric behavior with respect to the normal plane through $\varphi = 0$ (Fig. 1) could be excluded. Hence, the analysis was restricted to a 180° panel with symmetry conditions enforced at $\varphi = 0,\pi$. A uniform finite difference grid was chosen with 11 points in the axial and 29 points in the circumferential directions. Results obtained with finer grids indicated that use of the chosen grid led to accurate computations of the collapse load.

Due to the symmetry of the prebuckling deformation about the plane at midlength and about the normal plane through $\varphi = \pi/2$, it was necessary to excite nonsymmetric deformations by the use of small antisymmetric imperfections. Despite the presence of these imperfections a deformation pattern developed at collapse which was symmetric about both of these planes. Therefore, the continued analysis was

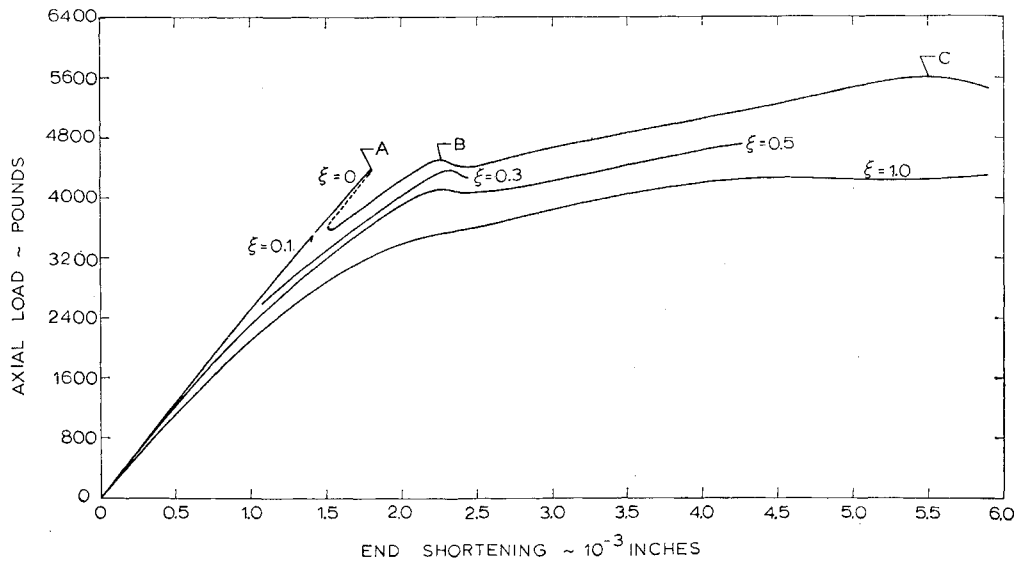

Fig. 2 Load-displacement curves for elliptic cylinders.

restricted to panels covering half the cylinder length and one quarter of the circumference.

For the particular cylinder considered (aspect ratio of 1.85) it is possible to determine the critical load without the use of symmetric (with respect to the geometric symmetry planes) imperfections. As the load is increased, a very sharp maximum is found in the load displacement curve (Fig. 2). Beyond this maximum convergence cannot be obtained, hence the postbuckling curve cannot be directly determined.

For an imperfect shell, the displacement mode which developed at collapse for a perfect shell was used as a guide in the choice of a suitable initial imperfection mode

$$\bar{w} = -w_0 \sin(\pi x/L) \cos(6\theta)$$

Load displacement curves were computed for several different values of the imperfection amplitude w_0. The results are shown in Fig. 2. The normal displacement at $\varphi = \pi/2$, $x = L/2$ is shown as a function of the axial load in Fig. 3. From Fig. 2 it can be seen that for a sufficiently large imperfection amplitude, the first sharp maximum does not exist—the curve is smooth and it is possible to find equilibrium configurations in the postbuckling range. After such configurations have been found they can be used as starting values for an analysis in which the imperfection amplitude is gradually changed until a point is found on the postbuckling curve for perfect shells. After such a point is found it is easy to establish postbuckling load displacement curves for perfect shells (Fig. 2).

After the first sharp maximum the postbuckling curve exhibits two additional limit points which correspond to secondary buckling. The curve was not pursued beyond the third maximum, because the deformations are then so large that the applicability of the basic equations is questionable. Also the buckle pattern is close to the point of maximum curvature, and bifurcation into an antisymmetric mode is likely. The normal displacement as a function of the circumferential arc length at $x = L/2$ is shown in Fig. 4. Curves are given for each of the three limit points.

In the neighborhood of a limit point the developing collapse or buckle mode can be obtained as the difference between displacements for two neighboring solutions. Such collapse modes corresponding to each of the three points of maximum are shown in Fig. 5. It can be seen that the point of maximum deflection in these patterns moves towards the point of maximum curvature as the end shortening increases. While the primary buckling load is rather sensitive to imperfections it appears that the second maximum is not imperfection, sensitive; hence, it may be suitable as a design limit. Results similar to these have been presented by Kempner et al., for oval shells.[5,6] However, Kempner's shells are not elliptic, and a direct comparison is not possible.

A series of elliptic cones was also analyzed. Like the cylinders, the cones were loaded through uniform axial shortening. At the two ends, rotation was unrestrained but the

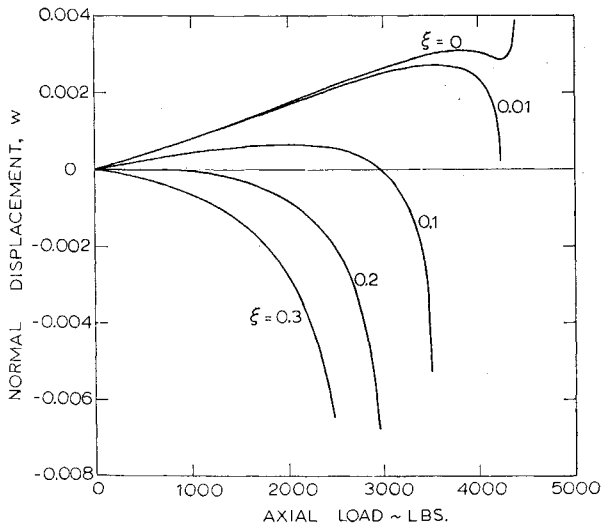

Fig. 3 Normal displacement vs axial load.

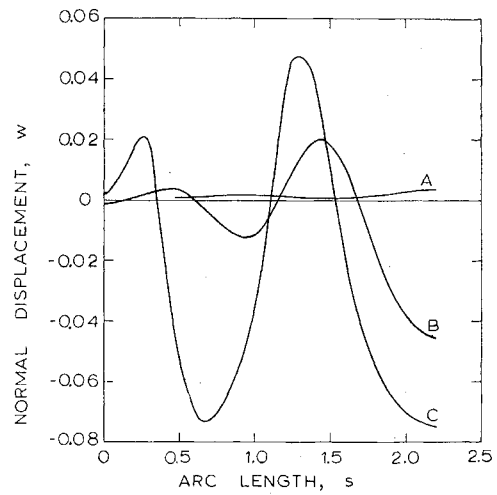

Fig. 4 Normal displacement patterns at the limit points.

Table 1 Dimensions of the elliptic cones

Case	$\bar{a} \cdot c$ in.	$\bar{b} \cdot c$ in.
1	10.65	10.65
2	11.9	9.5
3	12.2	8.7
4	13.0	7.4

cross section was not allowed to deform. Four different cases (including a circular cone) were analyzed. The aspect ratio of the elliptic cross section was varied, but the semiaxes of the ellipse were chosen such that the circumference was the same in all cases. Young's modulus was chosen to be 10^7 psi and Poisson's ratio was 0.3. All the cones had the dimensions (Fig. 1) $t = 0.16$ in., $c = 16$ in., and $d = 16$ in. The dimensions of the ellipse are shown in Table 1.

The results for the elliptic cylinders indicate that an imperfection with an amplitude of about 1% of the shell thickness will not significantly change the critical load. However, if this imperfection is included, a less severe convergence criterion may be used. Consequently, for economy in the analysis such an imperfection was included here. Figure 6 shows how the critical load varies with the ellipse ratio for elliptic cones of equal weight. The decrease in buckling load with increasing aspect ratio is less drastic than is indicated by the bifurcation buckling analysis for oval cylinders.[5] This may be partly caused by the fact that the elliptic geometry is more favorable than the one considered by Kempner and Chen. Also it appears that bifurcation in the linearized analysis occurs at a lower load and is followed by an increase in load until a maximum occurs. For the circular cone the bifurcation point and the maximum coincide, but for higher values of the aspect ratio the critical load is well above the bifurcation point. The buckling mode for case 3 ($\bar{a}/\bar{b} = 1.4$) is shown in Fig. 7.

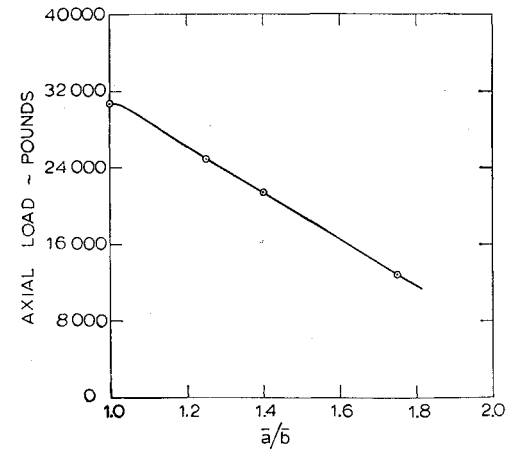

Fig. 6 Buckling loads for elliptic cones.

It must be emphasized that for all the cases investigated here a uniform end shortening was applied to the shell. Had a uniformly distributed axial load been applied at both edges, the possibilities for redistribution of stresses would have been limited and the performance of the elliptic shells would have compared less favorably to shells with circular cross section.

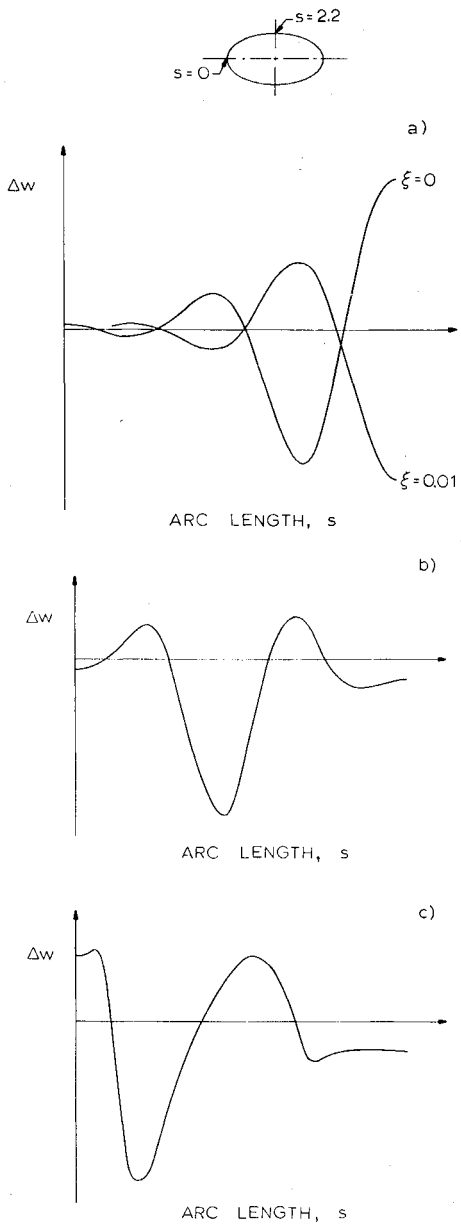

Fig. 5 Buckling patterns at a) point *A*, b) point *B*, c) point *C*.

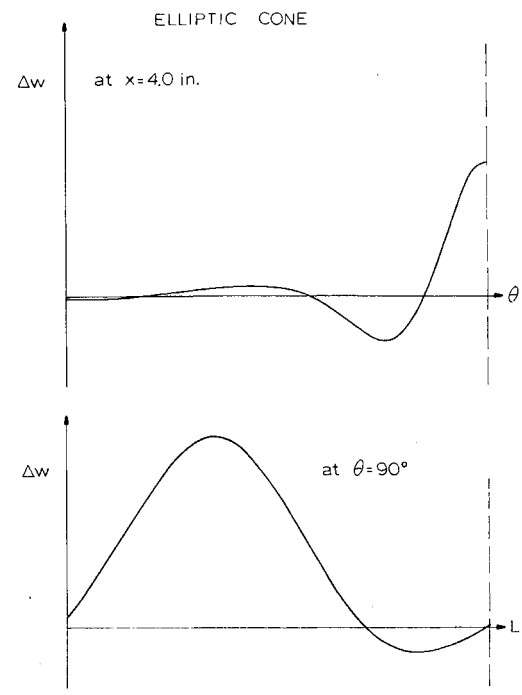

Fig. 7 Buckling patterns for elliptic cones; a) at $x = L/2$, b) at $\varphi = \pi/2$.

References

[1] Brogan, F. and Almroth, B. O., "Buckling of Cylinders with Cutouts," *AIAA Journal*, Vol. 8, No. 2, Feb. 1970, pp. 236–240.

[2] Stricklin, J. A. et al., "Linear and Nonlinear Analysis of Shells of Revolution with Asymmetric Stiffness Properties," *Proceedings of the Second Conference on Matrix Methods of Structural Mechanics*, AFFDL TR-69, Oct. 1968, Wright-Patterson Air Force Base, Ohio.

[3] Marlowe, M. B. and Flügge, W., "Some New Developments in the Foundations of Shell Theory," LMSC-6-78-68-13, May 1968, Lockheed Missiles & Space Company, Palo Alto, Calif.

[4] Sanders, J. L., Jr., "Nonlinear Theories for Thin Shells," *Quarterly of Applied Mathematics*, Vol. 21, No. 1, 1963, pp. 21–36.

[5] Kempner, J. and Chen, Y.-N., "Buckling and Postbuckling of an Axially Compressed Oval Cylindrical Shell," *Symposium on the Theory of Shells to Honor Lloyd Hamilton Donnell*, McCutchan Publishing Corp., Univ. of Houston, May 1967, pp. 141–183; also PIBAL Rept. 917, Polytechnic Institute of Brooklyn.

[6] Kempner, J. and Chen, Y.-N., "Postbuckling of an Axially Compressed Oval Cylindrical Shell," *Proceedings of the 12th International Congress of Applied Mechanics*, Aug. 26–31, 1968, Stanford Univ., Palo Alto, Calif., pp. 246–268; also PIBAL Rept. 68-31, Polytechnic Institute of Brooklyn.

JANUARY 1971 AIAA JOURNAL VOL. 9, NO. 1

Cylindrical Shell with an Axisymmetric Moving Load

K. SCHIFFNER*

Institut für Festigkeit, Deutsche Forschungs-und Versuchsanstalt für Luft-und Raumfahrt E.V., Mülheim/Ruhr, Germany

AND

C. R. STEELE†

Stanford University, Palo Alto, Calif.

The transient response of a semi-infinite, simply-supported cylindrical shell caused by an axisymmetrically engulfing, step pressure wave is investigated. Equations including the effects of transverse shear deformtion and rotary inertia are used. The rather involved contour integral solution to the problem is evaluated by means of modified saddle-point methods in terms of the Fresnel integrals and the integral of the Airy function. As expected, for load velocities smaller than the shear wave velocity of the shell material, the cylinder response is found to be analogous to that for an Euler-Bernoulli beam on an elastic foundation. Thus a load velocity equal to the minimum phase velocity is a "critical" velocity; i.e., the response increases with the square root of the distance of the load front from the end of the cylinder and, so, can become of large magnitude for practical problems of long cylinders with little damping. For the high load velocities, the short wavelength portion of the response is analogous to that for a Timoshenko beam on an elastic foundation, for which no further "critical" velocities occur, even at the "shear" and "bar"—which for the cylinder becomes the "plate"—velocities. However, in the long wavelength portion of the response of the cylinder, the transition from "bending" to axial "membrane" behavior causes the "bar" velocity to also be critical.

Introduction

PROBLEMS involving the transient response of structures to moving loads have attracted a number of investigators who have utilized various approaches. However, for the long cylinder the direct finite element, finite difference, or modal superposition numerical methods are not advantageous because of the localized nature of the transient response. To take advantage of this nature, the relatively simple "steady-state" solution, which depends only on the distance from a moving load discontinuity, has been utilized, as in the investigations by Jones and Bhuta,[1] and Herrmann and Baker.[2] This steady-state solution indicates that unbounded response occurs at four "critical" load speeds. These are equal to 1) the speed of disturbance propagation in a flat plate, 2) the slightly lower speed of propagation in a bar, 3) the speed of shear waves, and 4) the substantially lower minimum phase velocity for the cylinder.

In order to understand the significance of the steady-state solution in general and the actual behavior at the critical load speeds in particular, the transient response of the semi-infinite beam on an elastic foundation, which is analogous to the cylinder in many respects, was investigated. In Ref. 3, the response of the Euler-Bernoulli beam was found to increase with the square root of the distance of the load discontinuity from the beam end when the load speed equaled the minimum phase velocity, which qualifies this load speed to be referred to as critical. However, in the investigation of the Timoshenko beam,[4] it was found that, although the solution never achieves a "steady-state," the response to a load moving at the shear and bar velocities was bounded; so these speeds are not actually critical.

Thus, with a background of work on the analogous, but considerably simpler beam problems, we come to the present task of investigating the transient response of the cylinder. In particular, we seek a resolution to the question of which of the four speeds, at which the steady-state solution does not exist, are actually critical load speeds.

Since the high load speeds are of interest, equations including the effect of transverse shear deformation and rotary iner-

Presented as Paper 70-18 at the AIAA 8th Aerospace Sciences Meeting, New York, January 19–21, 1970; submitted November 7, 1969; revision received May 4, 1970.

* Abteilungsleiter, Abteilung Statik und Dynamik; NASA University Fellow for 1968/69 at Stanford University.

† Associate Professor of Aeronautics and Astronautics. Stanford University. Member AIAA.